Cell Reports, Volume *34*

Supplemental information

Hedgehog signaling and Tre1 regulate actin dynamics through $PI(4,5)P_2$ to direct migration of *Drosophila* embryonic germ cells

Ji Hoon Kim, Caitlin D. Hanlon, Sunaina Vohra, Peter N. Devreotes, and Deborah J. Andrew

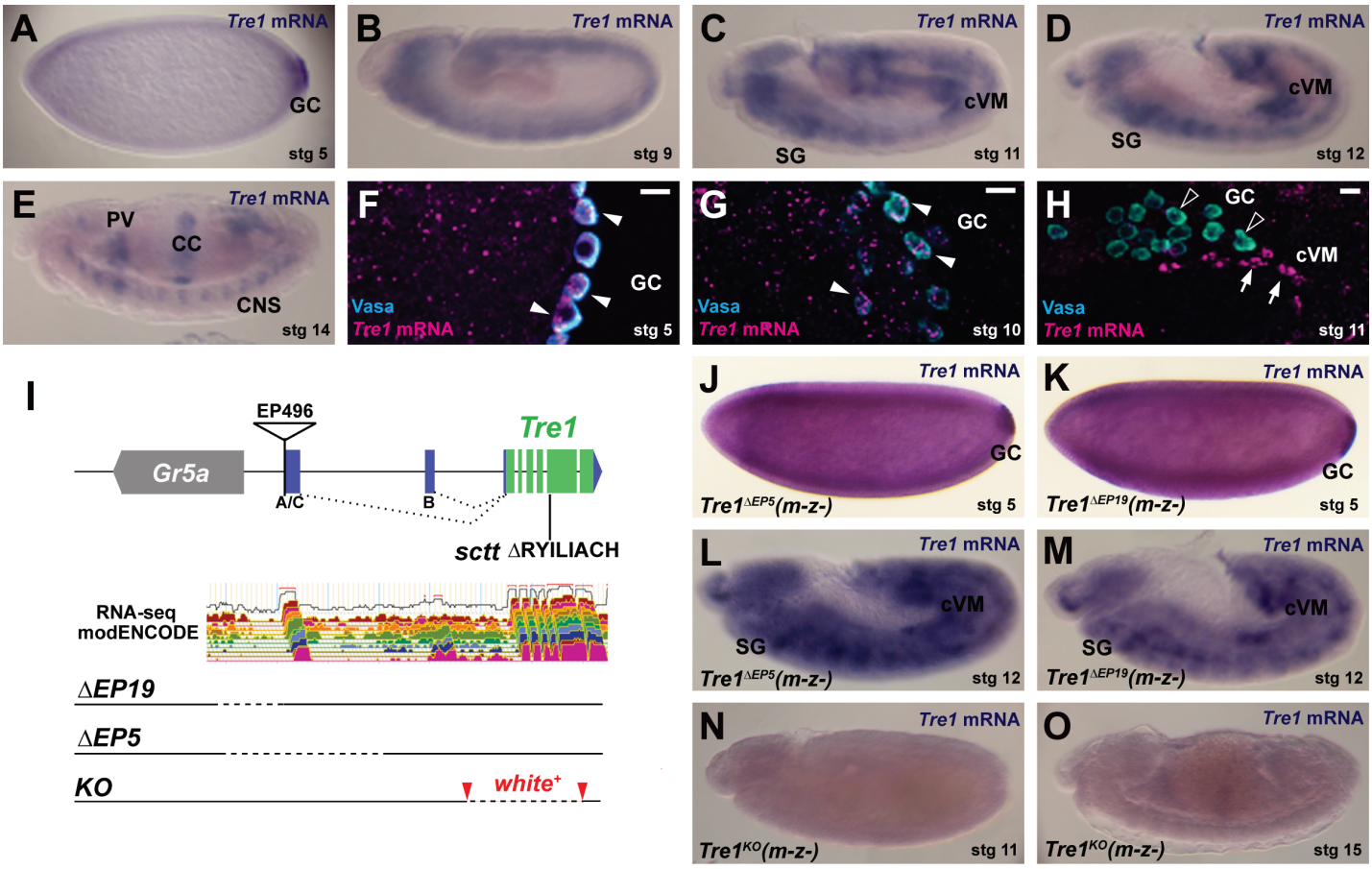

Figure S1. Expression of *Tre1* in Drosophila embryos and Generation of a Tre1 null allele by homologous recombination. (A-E) in situ hybridization revealed *Tre1* mRNA expression in GCs, caudal visceral mesoderm (cVM), salivary gland (SG), proventriculus (PV), copper cells (CC) and central nervous system (CNS) in stage (stg) 5 – 14 embryos. (F-H) *Tre1* mRNA in GCs (F,G) and cVM (H) visualized by fluorescent in situ hybridization. GCs were marked by Vasa staining. (F,G) Tre1 mRNA is present in the GCs up through the time when they exit the endoderm during stage 10. (H) *Tre1* mRNA is no longer detected in GCs for most of their migration; the nearby signals observed at stage 11 correspond to expression in the caudal visceral mesoderm. Nonetheless, bioinformatic analysis estimates that the corresponding Tre1 protein would remain present for the duration of GC migration (Expasy ProtParam). Scale bars, 10 μm. (I) *Tre1* gene structure. Existing Tre1 alleles include two derived from the excision of P

element EP496 (ΔEP19 and ΔEP5) and one (*sctt*) that deletes eight residues including the RY residues of the critical NRY motif. A null allele in which the entire ORF is replaced with the *white+* eye color gene was generated using homologous recombination. Dotted lines indicate region deleted. (J-O) *Tre1* mRNA in situ hybridization. The ΔEP19 and ΔEP5 alleles make easily detectable *Tre1* transcript in GCs (J,K) and other tissues (L,M), whereas the KO allele does not (N,O). Related to Figure 1.

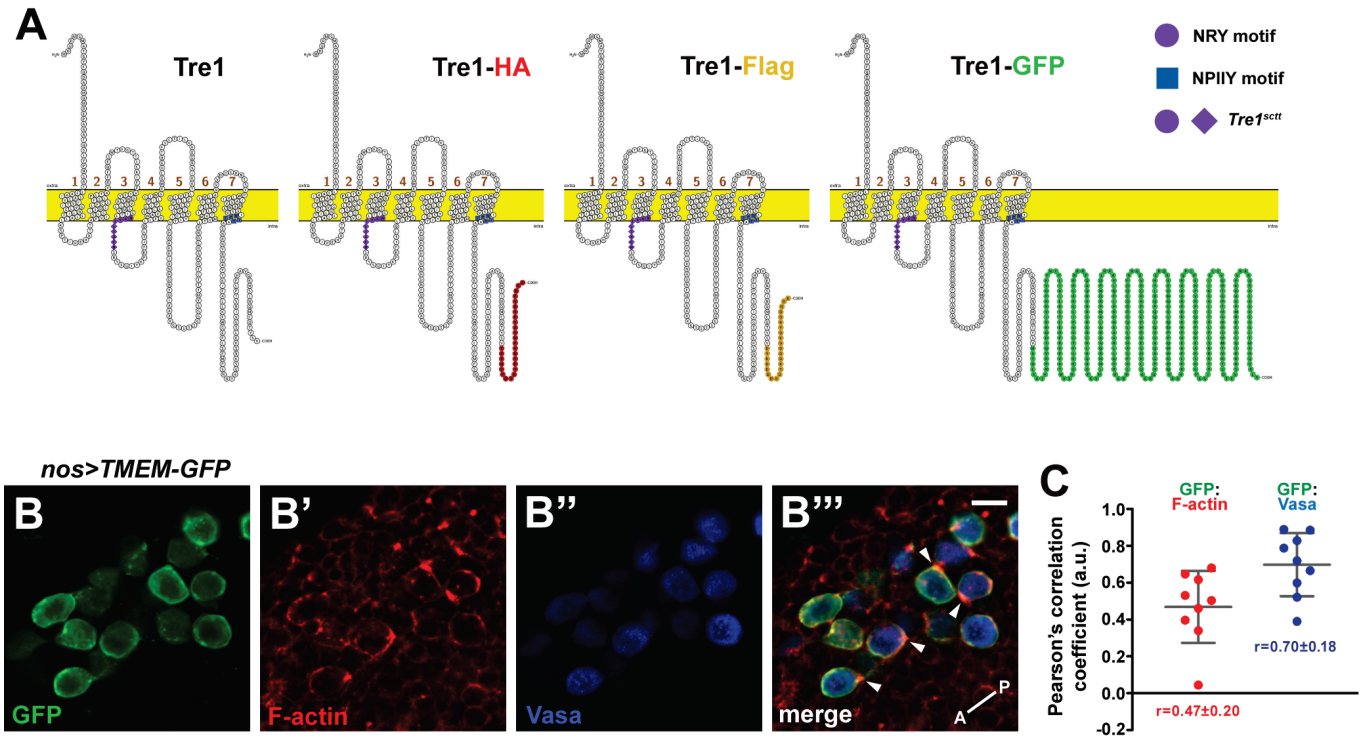

Figure S2. Ribbon diagrams of untagged and C-terminally tagged versions of Tre1, showing motifs and relative lengths of the different tags. (A) Cartoons show the ribbon structure of Tre1 and the relative length of the C-terminal tags HA (red), FLAG (gold), and GFP (Green). Yellow indicates the plasma membrane. Outside the cell is up, inside is down. Also indicated are the NRY motif (purple filled circles) and the NPIIY motif (blue squares). The *Tre1*^{sctt} allele deletes the NRY domain (purple filled circles) and a few nearby residues (purple filled diamonds). (B-B''') GCs with nos-Gal4 driven expression of a plasma membrane marker TMEM-GFP stained for GFP (B), F-actin (B'), VASA (A") and merge (B'''). Note that GFP signals (green) are not proportionally increased with F-actin signals (red) at protrusions (arrowheads) in comparison with other plasma membrane areas. The embryo in dorsal view and the A-P axis indicated. (C) The Pearson's correlation coefficients between fluorescent signals from GC boundaries in B'''. Related to Figure 2.

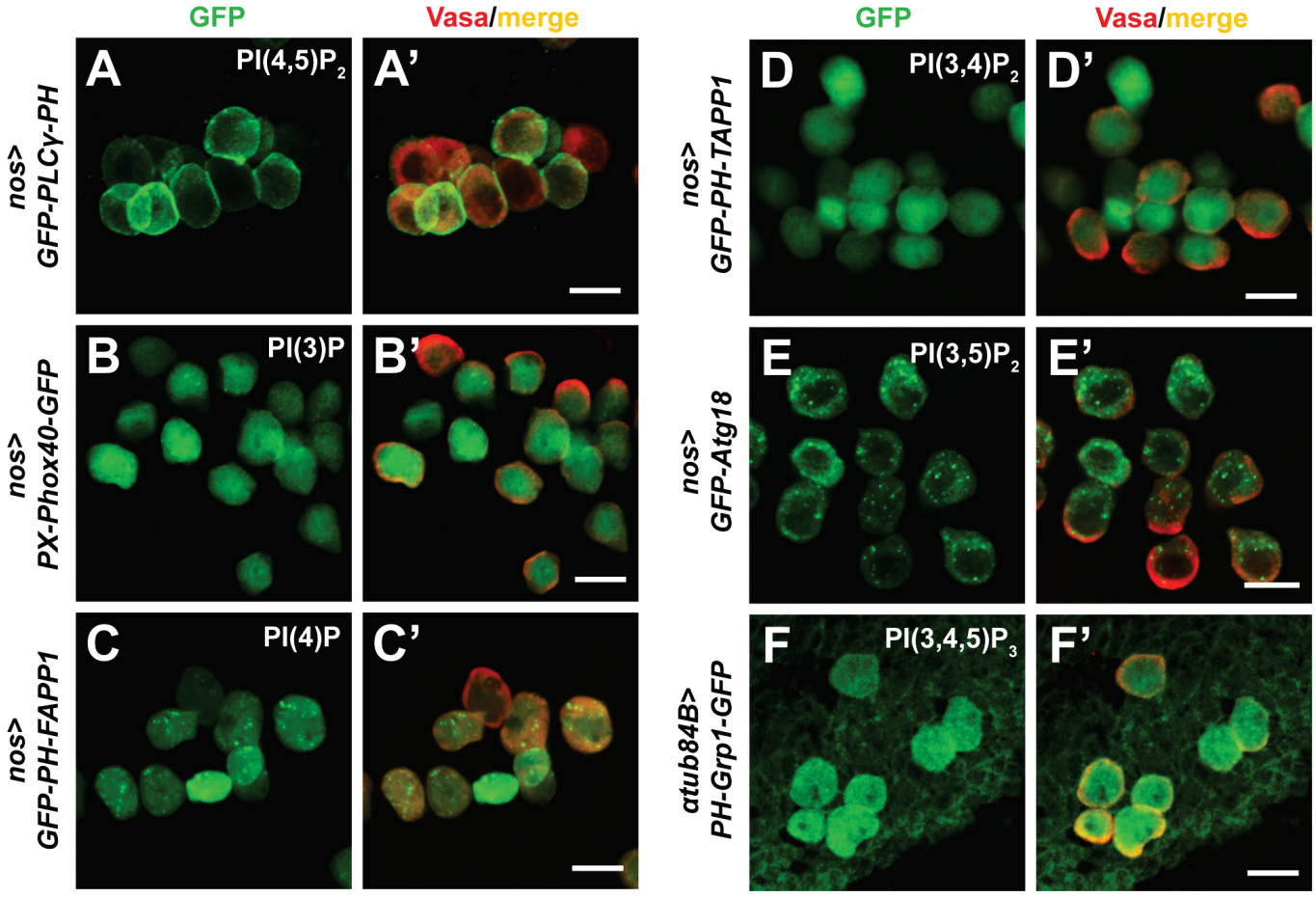

Figure S3. PI sensors localize to different cellular domains in migrating GCs. (A-F') GC (stained with Vasa, red) expression of GFP-tagged phosphoinositide sensors driven by nos-Gal4. (A-A') GFP-PLCγ-PH, a $PI(4,5)P_2$ sensor. (B-B') PX-Phox40-GFP, a PI(3)P sensor. (C-C') GFP-PH-FAPP1, a PI(4)P sensor. (D-D') GFP-PH-TAPP1, a $PI(3,4)P_2$ sensor. (E-E') GFP-ATG18, a $PI(3,5)P_2$ sensor. (F-F') PH-Grp1, a $PI(3,4,5)P_3$ sensor. All GC images are from st 11 embryos. Scale bars, 10 μm. Related to Figure 2.

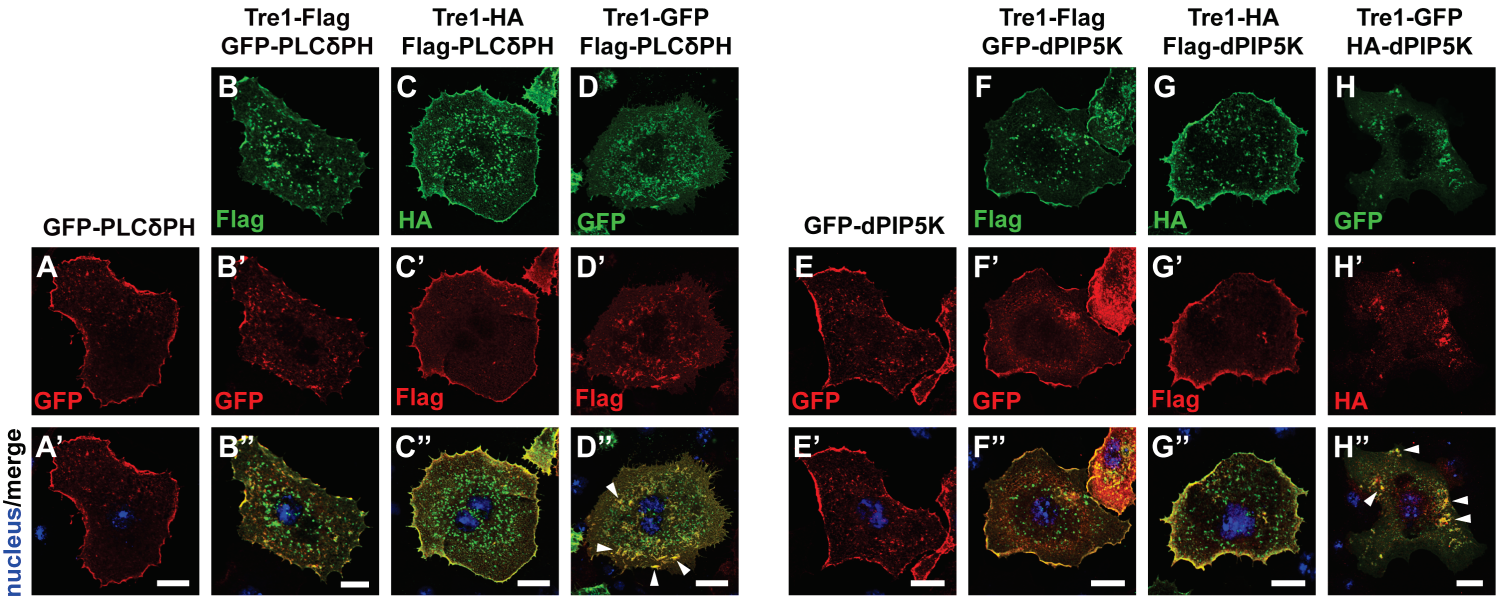

Figure S4. PI(4,5)P_2 sensor and dPIP5K colocalize with Tre1-GFP in large intracellular punctae but colocalize with Tre1-Flag or Tre1-HA only at the plasma membrane. (A-D'') Colocalization of the PI(4,5)P_2 sensor is seen with plasma-membrane localized Tre1-Flag and Tre1-HA, whereas colocalization is observed in large intracellular puncta with Tre1-GFP (arrowhead in D''). (E-H'') Colocalization of the dPIP5K is seen with plasma-membrane localized Tre1-Flag and Tre1-HA, whereas colocalization is observed in large intracellular puncta with Tre1-GFP (arrowheads in H''). Scale bars, 10 μm. Related to Figure 2.

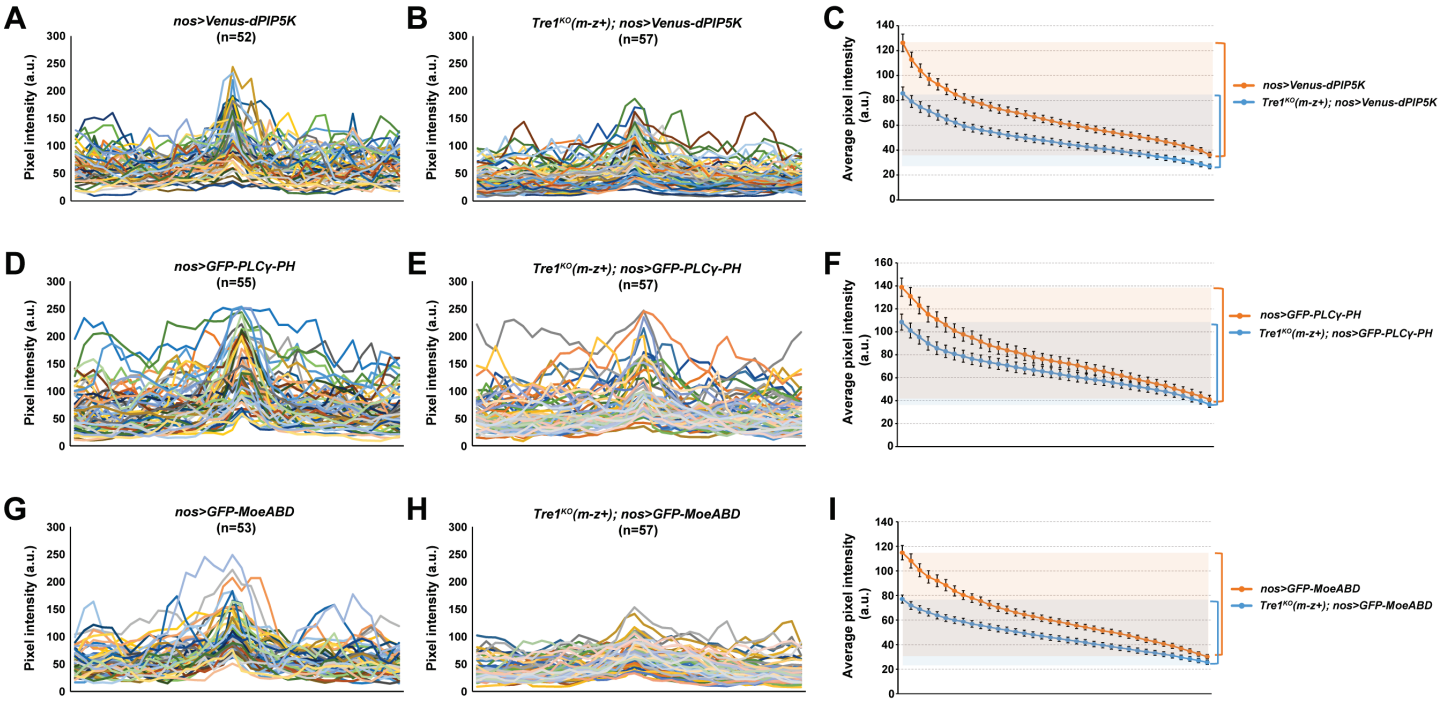

Figure S5. *Tre1* mutant GCs display decreased polarization of dPIP5K, PI(4,5)P_2 and F-actin. The line scans of fluorescent intensity of Venus-dPIP5K (A,B), GFP-PLCγPH (D,E), and GFP-MoeABD (G,H) from individual GCs are presented. Note that the majorities of WT GCs (A,D,G) display a single prominent peak whereas less peaks are present in *Tre1* mutant GCs (B,E,H). (C,F,I) The average intensity of fluorescent signals is aligned from the highest to the lowest. The ranges from the highest to the lowest points are greater in WTs (orange line) than in *Tre1* mutants (blue line) indicating that *Tre1* mutant GCs do not have high local concentrations of dPIP5K, PI(4,5)P_2 and F-actin. Error bars represent standard deviation. Related to Figure 3.

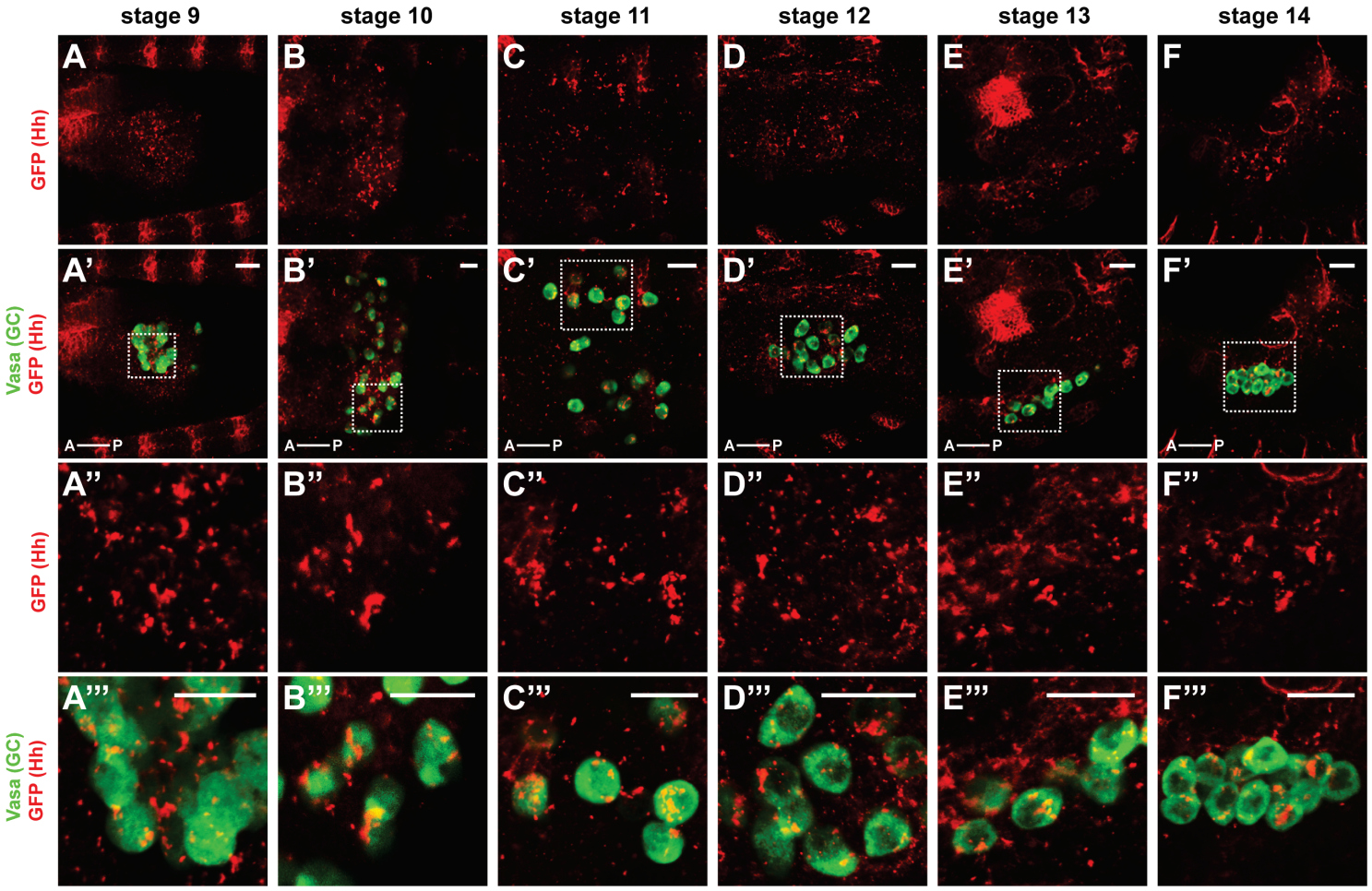

Figure S6. Hh expression through stages of GC navigation. GFP-tagged Hh proteins were expressed from a Bac transgene recapitulating the endogenous expression and stained with anti-GFP antibody (red). GCs were visualized by anti-Vasa staining (green). The boxed area in A'-F' were magnified in A''-F''', correspondingly. All images are a single optical slice and were taken in dorsal view. The A-P axis indicated. Scale bars, 20 μm. Related to Figure 5.

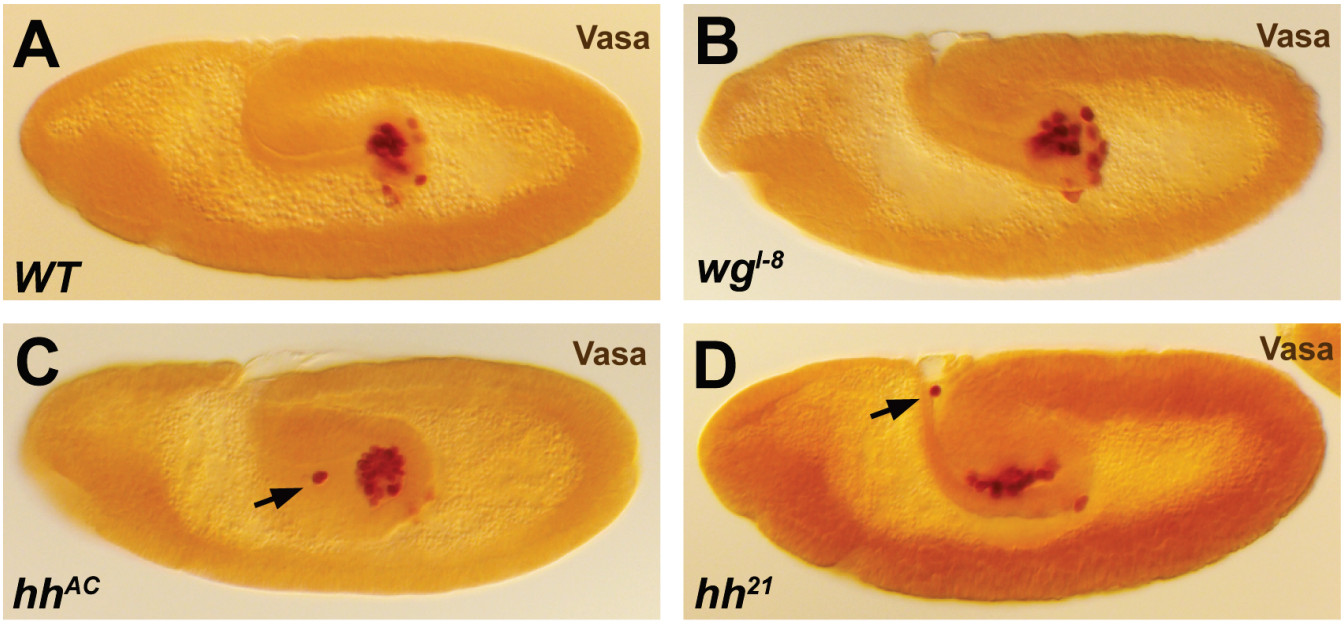

Figure S7. Early GC navigation defect in *hh* mutant embryos. (A) Vasa staining in a WT stage 10 embryo. (B-D) Vasa staining in stage 10 embryos mutant for *wg* (B) or *hh* (C,D). Black arrows highlight early mis-migrating GCs. Related to Figure 6.

	WT	Tre1^{KO} X Tre1^{KO}/Y (m-z-)	Tre1^{KO} X GFP*/Y (m-z+)	Tre1^{KO}/lacZ X Tre1^{KO}/Y (m+z-)	Tre1$^{\Delta EPS/KO}$ X Tre1^{KO}/Y (m-z-)	Tre1$^{scit/KO}$ X Tre1^{KO}/Y (m-z-)	Tre1^{KO}(m-z-); nos-Gal4	Tre1^{KO}(m-z-); UAS-Tre1	Tre1^{KO}(m-z-); nos>Tre1	Tre1^{KO}(m-z-); nos>Tre1-HA	Tre1^{KO}(m-z-); nos>Tre1-Flag	Tre1^{KO}(m-z-); nos>Tre1-GFP	nos>Tre1-FLAG	nos>Tre1-GFP
WT		687.79	450.759	10.106	655.487	790.002	329.245	365.411	32.618	149.107	61.36	279.705	7.206	224.112
Tre1^{KO} X Tre1^{KO}/Y (m-z-)	4.40E-150		0.937	470.532	3.395	22.438	25.539	1.522	340.886	230.636	267.131	29.58	376.444	48.155
Tre1^{KO} X GFP*/Y (m-z+)	1.32E-98	0.626		325.382	5.903	22.153	11.946	0.933	239.554	142.601	181.117	15.975	273.385	26.291
Tre1^{KO}/lacZ X Tre1^{KO}/Y (m+z-)	0.00639	6.69E-103	2.21E-69		463.208	565.849	310.149	62.047	6.719	75.994	23.484	186.384	2.243	154.654
Tre1$^{\Delta EPS/KO}$ X Tre1^{KO}/Y (m-z-)	4.60E-143	0.183	0.52	2.11E-101		9.373	37.9	4.634	345.781	238.185	275.021	41.359	380.188	61.599
Tre1$^{scit/KO}$ X Tre1^{KO}/Y (m-z-)	2.84E-172	0.000013	0.000015	1.34E-123	0.009217		69.723	21.995	432.006	332.824	353.762	75.626	458.602	95.021
Tre1^{KO}(m-z-); nos-Gal4	3.20E-72	2.85E-06	0.002547	5.89E-09	5.89E-09	7.24E-16		13.507	154.494	70.462	105.936	1.755	187.929	3.946
Tre1^{KO}(m-z-); UAS-Tre1	4.49E-80	0.467	0.627	9.90E-02	0.099	0.000017	0.001167		228.523	131.832	172.679	15.491	264.078	28.85
Tre1^{KO}(m-z-); nos>Tre1	8.26E-08	9.49E-75	9.60E-53	0.035	8.22E-76	1.55E-94	2.83E-34	2.38E-50		35.557	6.66	126.922	9.022	105.563
Tre1^{KO}(m-z-); nos>Tre1-HA	4.19E-33	8.28E-51	1.08-31	3.15E-17	1.90E-52	5.30E-73	5.00E-16	2.36E-29	1.90E-08		12.277	48.762	66.919	38.451
Tre1^{KO}(m-z-); nos>Tre1-Flag	4.73E-14	9.84E-59	4.69E-40	7.95E-06	1.91E-60	1.52E-77	9.92E-24	3.19E-38	0.36	0.002159		84.109	25.249	65.899
Tre1^{KO}(m-z-); nos>Tre1-GFP	1.83E-61	3.77E-07	0.00034	3.37E-41	1.04E-09	3.78E-17	0.412	0.000433	2.75E-28	2.58E-11	5.44E-19		161.836	4.342
nos>Tre1-FLAG	0.027	1.80E-82	4.32E-60	0.326	2.77E-83	2.61E-100	1.56E-41	4.53E-58	0.011	2.94E-15	3.29E-06	7.10E-36		135.31
nos>Tre1-GFP	2.16E-49	3.49E-11	1.43E-06	2.61E-34	4.21E-14	2.32E-21	0.139	5.44E-07	1.19E-23	4.47E-09	4.90E-15	0.114	4.15E-30	

Supplementary Table Set 1. Statistical analyses of phenotypes in GC migration with different *Tre1* mutant conditions are shown. Related to Figure 1.

	WT	dpip5k^{18}	dpip5k^{30}	dpip5k^{18}, sktl$^{\Delta 15}$	matαtub>dpip5kRNAi^{HMC05328}	matαtub>sktlRNAi^{GL00072}	tre1^{KO}/+; UAS-HA-dPIP5K^{KD}	nos>HA-dPIP5K^{KD}	tre1^{KO}/+; nos>HA-dPIP5K^{KD}
WT		2.261	0.963	4.263	61.964	1.156	0.00142	1.174	27.136
dpip5k^{18}	0.323		3.445	0.721	56.827	5.524	1.916	1.397	28.016
dpip5k^{30}	0.618	0.179		5.307	27.34	0.044	0.801	3.329	10.512
dpip5k^{18}, sktl$^{\Delta 15}$	0.119	0.697	0.492		39.87	7.578	3.784	2.259	22.658
matαtub>dpip5kRNAi^{HMC05328}	3.50E-14	4.57E-13	1.16E-06	2.20E-09		65.635	50.146	62.403	8.312
matαtub>sktlRNAi^{GL00072}	0.561	0.063	0.978	0.023	5.59E-15		0.865	4.383	23.982
tre1^{KO}/+; UAS-HA-dPIP5K^{KD}	0.999	0.384	0.67	0.151	1.29E-11	0.649		1.106	22.313
nos>HA-dPIP5K^{KD}	0.556	0.497	0.189	0.323	2.81E-14	0.112	0.575		31.645
tre1^{KO}/+; nos>HA-dPIP5K^{KD}	1.28E-06	8.25E-07	0.005216	0.000012	0.016	6.20E-06	0.000014	1.34E-07	

Supplementary Table Set 2. Statistical analyses of phenotypes in GC migration with *dpip5k* and *sktl* loss of functions are shown. Related to Figure 2.

	WT	$wasp^{1}$	$wasp^{3}$	$wasp^{1}/wasp^{3}$	$dpip5k^{18}$	$dpip5k^{18}$; $wasp^{1}/wasp^{3}$	$dwip^{S1946}$	$dwip^{S1946}$/Df(2R)Exel7170
WT		206.8	152.49	135.303	2.261	146.434	43.229	36.986
$wasp^{1}$	1.20E-45		5.358	51.853	184.333	4.202	122.032	89.936
$wasp^{3}$	7.71E-34	0.069		19.405	136.938	71.244	51.853	52.544
$wasp^{1}/wasp^{3}$	4.16E-30	5.50E-12	0.000061		0.66	121.767	35.057	22.755
$dpip5k^{18}$	0.323	9.39E-41	1.84E-30	3.20E-27		133.238	40.846	35.805
$dpip5k^{18}$; $wasp^{1}/wasp^{3}$	1.59E-32	0.122	0.719	0.000087	1.17E-29		68.58	52.721
$dwip^{S1946}$	4.10E-10	3.17E-27	3.39E-16	2.44E-08	1.35E-09	1.28E-15		0.084
$dwip^{S1946}$/Df(2R)Exel7170	9.30E-09	2.96E-20	3.89E-12	0.000011	1.68E-08	3.56E-12	0.959	

Supplementary Table Set 3. Statistical analyses of phenotypes in GC migration with *wasp* and *dwip* mutant conditions are shown. Related to Figure 4.

	WT	hh[Mrt]/+	SmoRNAi^{HMC03577}	matαtub>SmoRNAi^{HMC03577}	SmoRNAi^{GL01472}	matαtub>SmoRNAi^{GL01472}	nos-Gal4	UAS-GFP-Ptc	nos>Smo-GFP	nos>GFP-Ptc
WT		120.943	15.272	191.907	3.1	126.971	0.015	2.041	0.05	72.91
hh[Mrt]/+	5.47E-27		38.898	16.352	74.964	6.695	105.848	87.408	101.17	15.124
SmoRNAi^{HMC03577}	0.000483	3.58E-09		86.391	4.959	55.6	13.136	8.403	12.223	12.732
matαtub>SmoRNAi^{HMC03577}	2.13E-42	0.000281	1.74E-19		133.928	0.76	171.797	149.383	165.689	61.936
SmoRNAi^{GL01472}	0.212	5.27E-17	0.084	8.20E-30		89.074	2.453	2.524	2.11	37.692
matαtub>SmoRNAi^{GL01472}	2.68E-28	0.035	8.44E-13	0.684	4.55E-20		115.235	98.631	111.433	31.928
nos-Gal4	0.992	1.04E-23	0.001404	4.95E-38	0.293	9.49E-26		1.679	0.00959	61.909
UAS-GFP-Ptc	0.36	1.05E-19	0.015	3.65E-33	0.283	3.82E-22	0.432		1.546	47.143
nos>Smo-GFP	0.975	1.07E-22	0.002217	1.05E-36	0.348	6.35E-25	0.995	0.462		58.432
nos>GFP-Ptc	1.47E-16	0.00052	0.001719	3.55E-14	6.54E-09	1.17E-07	3.60E-14	5.80E-11	2.05E-13	

Supplementary Table Set 4. Statistical analyses of phenotypes in GC migration associated with loss of *hh* and *smo* expression and overexpression of GFP-Smo or GFP-Ptc are shown. Related to Figure 6.